International Journal of Heat and Mass Transfer 216 (2023) 124600

Contents lists available at ScienceDirect

International Journal of Heat and Mass Transfer

journal homepage: www.elsevier.com/locate/ijhmt

Experimental assessment and predictive model of the performance of Ti-based nanofluids

Alessandro d'Adamo [a,b,*], Martino Diana [a], Giuseppe Corda [a], Antonio Cucurachi [a], Maria Cannio [a], Andrea Pellacani [a], Marcello Romagnoli [a,b], Enrico Stalio [a,b], Paolo E. Santangelo [c,d]

[a] Dipartimento di Ingegneria "Enzo Ferrari", Università degli Studi di Modena e Reggio Emilia, Modena, Italy
[b] Centro Interdipartimentale di Ricerca e per i Servizi nel settore della produzione, stoccaggio e utilizzo dell'Idrogeno H2-MO.RE, Modena, Italy
[c] Dipartimento di Scienze e Metodi dell'Ingegneria, Università degli Studi di Modena e Reggio Emilia, Reggio Emilia, Italy
[d] Centro interdipartimentale per la ricerca En&Tech, Reggio Emilia, Italy

ARTICLE INFO

Keywords:
Titania
Water
Heat exchanger
Global heat transfer coefficient
Flow regime
Figures of merit

ABSTRACT

The need for innovative propulsion technologies (e.g., fuel cells) in the mobility sector is posing a higher-than-ever burden on thermal management. When low operative temperature shall be ensured, dissipation of a significant amount of heat is requested, together with limited temperature variation of the coolant; mobile applications also yield limitations in terms of space available for cooling subsystems. Nanofluids have recently become one of the most promising solutions to replace conventional coolants. However, the prediction of their effectiveness in terms of heat-transfer enhancement and required pumping power still appears a challenge, being limited by the lack of a general methodology that assesses them simultaneously in various flow regimes. To this end, an experiment was developed to compare a conventional coolant (ethylene glycol/water) and a TiO_2-based nanofluid (1% particle loading), focusing on heat transfer and pressure loss. The experimental dataset was used as an input for a physical model based on two independent figures of merit, aiming at an *a priori* evaluation of the potential simultaneous gain in heat transfer and parasitic power. The model showed conditions of combined gain specifically for the laminar flow regime, whereas turbulent flows proved inherently associated to higher pumping power; overall, criteria are presented to evaluate nanofluid performance as compared to that of conventional coolants. The model is generally applicable to the design of cooling systems and emphasizes laminar flow regime as promising in conjunction with the use of nanofluids, proposing indices for a quantitative *a priori* evaluation and leading to an advancement with respect to an *a posteriori* assessment of their performance.

1. Introduction

One of the parameters governing heat transfer enhancement is the thermal conductivity of the fluids employed as coolants, among which distilled water, ethylene glycol/water mixture (EG/W) or engine oils are the most common choices for industrial applications (e.g., automotive, manufacturing). In fact, several solid materials feature thermal conductivity 1 - 3 orders of magnitude higher than that of liquids: for instance, copper thermal conductivity is about 400 W m^{-1} K^{-1}, whereas that of liquid water is lower than 1 W m^{-1} K^{-1}. Therefore, solid matter appears overall an effective candidate as the heat transfer medium, and fluids containing solid particles of a highly conductive material are expected to benefit from that characteristic; such a mixture embodies a coolant with augmented heat transfer performance, with its properties being tailored by selecting the solid material and the amount of particles dispersed within the fluid phase. Those fluids are known as nanofluids: two-phase suspensions, where the continuous phase is a fluid - typically a liquid - and the dispersed phase is a solid material in the form of ultrafine (i.e., nanoscale) particles. As one of the first sources available in the open literature, nanofluids were conceptualized by Choi and Eastman [1], where the benefit from higher effective thermal conductivity was pioneered to allow reducing the required pumping power for cooling and the size of heat exchangers even down to miniature devices, particularly attractive for applications where high heat load is combined with space constraints. However, assuming that nanofluids mainly yield an increase in thermal conductivity of the coolant, dominating all the

* Corresponding author at: Dipartimento di Ingegneria "Enzo Ferrari", Università degli Studi di Modena e Reggio Emilia, Via P. Vivarelli 10, 41125 Modena, Italy.
E-mail address: alessandro.dadamo@unimore.it (A. d'Adamo).

https://doi.org/10.1016/j.ijheatmasstransfer.2023.124600
Received 18 May 2023; Received in revised form 31 July 2023; Accepted 11 August 2023
Available online 24 August 2023

other properties being affected by the added nanoparticles, oversimplifies the involved mechanisms and disguises the need for a more complex evaluation of their effectiveness as cooling media.

The possibility of tailoring the coolant to a specific application and the potential for outperforming the properties of conventional coolants to enhance heat exchange opened an innovative research direction within heat transfer and materials science towards identifying nanofluids that could be used for a variety of applications [2]. Among them, nanofluids have recently been proposed as particularly promising for cooling of fuel-cell stacks, with specific reference to Polymer Electrolyte Membrane Fuel Cells (PEMFC): the importance of thermal management to keep the electrochemically active Membrane and Electrode Assembly (MEA) within a 65 - 80 °C temperature range is paramount to minimize the cell internal resistance, thus requiring a dedicated cooling subsystem. To investigate heat transfer in PEMFC cooling, the seminal works by Zakaria et al. [3,4] present an experimental setup, where a heating pad was used to reproduce heat generation by fuel cells, then introducing a PEMFC stack [5] and using Al_2O_3-EG/W nanofluids flowing in laminar regime. In those works, a unified Figure of Merit (FoM) is proposed to rationalize the increase in rate of heat flow and pumping power: the Advantage Ratio (AR); moreover, another FoM is introduced to combine heat transfer enhancement and performance drop: the Thermo-Electrical Ratio (TER). However, both are formulated as a ratio between normalized quantities, so even in the authors' opinion the same relative improvement necessarily depends on the weight used for any specific application, thus making a general guideline to apply AR or TER still in demand (e.g., as a function of nanofluid flow regime). In a similar manner, the use of nanofluids for cooling of internal combustion engines (ICEs) has proved very attractive, as reviewed by Sidik et al. [6]. Unfortunately, the lack of a consolidated validation led to somewhat inconsistent outcomes among the different studies considered in the survey. The uncertain gain in the various fields of application and the still undisclosed potential are the main reasons for the relatively low technology readiness of nanofluids. The hindrance against full penetration into industry mainly consists of inconsistency in preparation standards, longevity assessment, performance evaluation, environmental impact, and life cycle assessment (LCA) [7,8]. The relatively recent possibility of using non-spherical particles (e.g., cylinders, platelets, nanorods) has introduced additional promising pathways for cooling purposes, as well as an even more emphasized need for clear and unambiguous characterization [9,10]. With regard to preparation methods, the significance of recognized standards is specifically stressed out with respect to long-term stability [11].

The complexity of nanofluids behavior lies in their multiphase nature, which affects the entire spectrum of their thermophysical properties. A long-lasting debate is still ongoing about the efforts required to investigate the involved fundamental processes, as well as to support the use of nanofluids in engineering applications. The difficulty of considering the essential nature of nanofluids when assessing their suitability for a specific application is highlighted by classical thermodynamic models [12–14], all of which exhibit limitations, but all still necessary to support the engineering of nanofluids. As for the modeling of heat transfer through nanofluids, the ultrafine size of the suspended particles has led both experiment and numerical efforts to mainly rely on the assumption of single-phase flow: the transport of the suspended nanoparticles within the liquid medium can be effectively described by the same governing equations of a single-phase fluid, with its thermophysical properties being appropriately modified to account for the presence of the nanosuspension [15,16]. This approach allows simplifying the model, although any nanoscale-pertinent process is inherently simplified, hence challenging the application of a continuous model to the nature of the investigated fluid and opening the field for more complex two-phase mixture models [17]. However, any engineering approach mainly requires global thermodynamics-based correlations to implement nanofluids characteristics in the design workflow, hence a simplified and experiment-guided single-phase model is pursued in the present study. Density ρr and specific heat capacity c of the nanofluid are typically calculated as a volume-weighted average of the base fluid and of the particle properties, with *nf* and *bf* subscripts referring to nanofluid and base fluid, respectively, and p referring to the solid phase. The relevant formulations are expressed by Eqs. (1) and (2), where the volumetric particle loading (φ) practically acts as a weighting factor. It is worth mentioning that the volume-weighted relationship for density was experimentally validated by Pak and Cho [18] for Al_2O_3 and TiO_2 particle dispersion in liquid water, with concentration being as high as 4%.

$$\rho_{nf} = (1-\varphi)\cdot\rho_{bf} + \varphi\cdot\rho_p, \tag{1}$$

$$c_{nf} = (1-\varphi)\cdot c_{bf} + \varphi\cdot c_p. \tag{2}$$

Regarding thermal conductivity and dynamic viscosity, the open literature appears to generally agree on the former following an increase with the temperature, whereas it is acknowledged that the latter exponentially reduces with temperature. The values of both properties grow as nanoparticle loading increases [19], and for higher surface-to-volume ratio of the particles' shape (i.e., for reduced sphericity) [20]. As a recognized advantage of nanofluids, thermal conductivity is emphasized with respect to the base fluid; several correlations have been proposed to evaluate it quantitatively [21,22] and comprehensive reviews are currently available on the characterization of thermophysical properties of nanofluids [23,24]. Scaling laws for thermal conductivity and dynamic viscosity as functions of the base fluid properties were developed by Corcione [25], showing that results from multiple experiments on various nanofluids could be satisfactorily correlated, and excellent benchmarks of nanofluids thermal conductivity and measurement methods are reported in Buongiorno et al. [26] and Patel et al. [27], although for a limited selection of compositions. The increase in thermal conductivity [13] is generally attributed to a combination of: the higher conductivity of the suspended solid phase; the promoted Brownian motion of nanoparticles within the liquid phase, which flattens the temperature profile over the generic cross-section of the heat exchanger by transporting more energy in close proximity to the walls; the remarkably large surface-to-volume ratio of nanoparticles, which fosters heat transfer and the liquid layering of fluid molecules around solid particles, leading to a less random and solid-like molecular structure. The relative impact of each of these mechanisms is still controversial, although their role is recognized in yielding thermal conductivity higher than that of the base fluid.

The relationship between flow regime and heat transfer in nanofluids has been the subject of extensive research and a considerable body of literature focuses on convective heat transfer coefficient and pressure losses as the main parameters embodying that relationship. Even though the details of the involved physical process are still somewhat obscure, since they depend on several factors (e.g., the molecular interaction between solid particles and the liquid phase, etc.), the general observation consists of nanofluids yielding an increase in both rate of heat flow and pressure loss. The former is substantiated by the higher thermal conductivity of the fluid itself and on an increase in the Nusselt number (Nu), whereas the latter is overall founded on the higher density and viscosity exhibited by nanofluids over the employed base fluid. Correlations suitable for predicting the Nusselt number of nanofluids (Nu_{nf}) were developed in several studies, generally showing an augmented convective heat transfer coefficient for nanofluids, as particle concentration is increased, with respect to that of base fluids flowing with the same Reynolds number (Re), i.e. $Re_{bf} = Re_{nf}$. As expected, the same trend can be observed under increased Re. The use of the Nusselt and Reynolds number as representative of heat transfer and flow regime aligns with the mentioned use of a single-phase effective model, provided that fluid-specific effective properties (e.g., dynamic viscosity, density, specific heat, thermal conductivity) be employed. For instance, Maïga et al. [16] focused on investigating heat transfer of Al_2O_3/water

and Al_2O_3/EG nanofluids by a numerical approach; both laminar and turbulent conditions under constant heat flux were considered in a 10 mm diameter and 1 m length tube, with the outcomes confirming the expected increase in heat transfer and in wall shear stress. Maïga et al. [28] further expanded their study to radial flow, and relationships for Nu_{nf} were obtained from numerical simulations for laminar conditions. Heat transfer and pressure loss increase were attributed to an enhanced near-wall mixing caused by the involved submicrometric particle-wall interaction [18]. The extensive review by Sarkar [29] summarizes several correlations for Nu_{nf} calculation for nanofluids in both laminar and turbulent flow regime, with the most relevant being reported in Table 1.

However, augmented heat transfer and pressure losses may not be considered as general features of nanofluids since they depend on the type and loading of the suspended particles, as well as on flow regime. Moreover, the difference between a comparison under the same velocity (i.e., the same volumetric flowrate) and a comparison under the same mass flowrate or *Re* shall be stressed out. This aspect becomes relevant, as while the nanoparticle concentration increases Nu_{nf} can potentially decrease with respect to that of the base fluid. This phenomenon is due to flow laminarization, which consists of a dominant increase in viscosity over that in density, thus reducing Re_{nf}. This observation demonstrates that a mere improvement in heat transfer performance by replacing a conventional coolant with nanofluids cannot be generally expected, and that an analysis is required of both the operating conditions (e.g., a comparative study of thermophysical properties and nanoparticle loading) and of the flow regime (e.g., tube diameter, Re_{nf}, Nu_{nf}), to evaluate the extent of benefit from employing them.

Among the multiple combinations of base fluid and solid suspended particles, an ethylene glycol/water mixture (EG/W) was selected, as it somewhat embodies an industrial standard among heat-transfer media, together with being the subject of several previous works that make its use rather substantiated. Notably, the EG/W mixture is a coolant typically employed for internal combustion engines and fuel cells [6], while a Ti-based nanofluids have been largely investigated [19,24,34], thus including them among those with the most consolidated background. Regarding nanofluid preparation, the dispersion of TiO_2 in an ethylene glycol/water mixture (TiO_2-EG/W) appears particularly relevant for the large-scale development of nanofluids, since the base fluid is a common coolant, the solution is not volatile or corrosive and it exhibits excellent long-term stability, thus preventing dispersion of ultrafine particles in the atmosphere. Therefore, the study presents an experimental comparison between EG/W and EG/W-TiO_2 in terms of cooling capabilities to support the development of a method to predict the respective gain or loss in heat transfer rate and pumping power. With regard to the thermophysical properties of TiO_2-EG/W nanofluids, Reddy and Rao [35] proposed a linear correlation for the thermal conductivity of TiO_2-EG/W nanofluids as based on dedicated experiments; however, the relationship is not mathematically continuous with the same property of the base fluid, as particle concentration approaches zero. Hamid et al. [36] experimentally tested TiO_2-EG/W nanofluids in an apparatus with constant heat flux at the walls, under turbulent flow regime, showing both an increase in heat transfer and in pressure drop to be balanced by pumping power. The same observations were found by Reddy and Rao [33], who evaluated Nu_{nf} and the friction factor (f_{nf}) for TiO_2-EG/W nanofluids - with and without helical coil inserts - in turbulent conditions. Similar results in terms of experimentally assessed Nu_{nf} is the study by Duangthongsuk and Wongwises [32], where it was observed that the relationship for thermal conductivity from Yu and Choi [22] is identified as that yielding the best approximation for TiO_2-based nanofluids.

Interestingly, the recent increase in scientific interest and contributions has not provided a validated general approach to predict the performance of nanofluids in terms of enhanced heat exchange and required pumping power. The extensive efforts spent to investigate their behavior have led to the proliferation of relationships for their thermophysical properties, friction factor and heat transfer coefficient; however, this has not yet resulted in a consolidated understanding of the involved physics and of the engineering perspective. This observation motivated the present research, where some response is provided to the following questions, still pending within the heat transfer community:

- a significant lack of predictive (i.e., *a priori*) indications about whether nanofluids are beneficial or not seems to require dedicated efforts, especially when considering both heat transfer and pumping power. Indeed, such evaluation, when currently available, is usually limited to *a posteriori* verification against a specific apparatus, thus missing a universal discussion to generalize the obtained results;
- in case the use of nanofluids leads to augment heat transfer, while not requiring an increased pumping power, the flow regime identifying those conditions appears still not fully investigated. Therefore, a physics-based framework to provide quantitative information in that regard would be quite relevant to provide guidance towards their effective application for cooling;
- the available literature on nanofluids is quite substantial, yet it presents sparse datasets in terms of type of base fluid (mostly water, EG/W and oil), type and shape of suspended particles (mostly TiO_2, CuO, SiO_2 and Al_2O_3) and their loading within the base fluid, preparation methods, thermophysical properties of interest, flow regime (i.e., laminar, turbulent) and standardized comparison between base fluid and nanofluid (e.g., under the same flowrate, the same *Re*). This amount of scattered data has made the scientific community focus primarily on obtaining results specific to selected configurations, rather than on pursuing outcomes of general validity for engineering purposes. In that regard, a remarkable advancement consists of the

Table 1
Correlations for estimating Nu_{nf} of nanofluids, selected from those currently available in the open literature.

Base fluid	Solid-particle material	Particle loading	Particle shape	Correlation	Range of applicability	Reference
Water	Cu	2.0 vol%	Spherical	$Nu_{nf} = 0.4328(1.0 + 11.285 \cdot \varphi^{0.754} \cdot Pe^{0.218}) \cdot Re_{nf}^{0.333} \cdot Pr_{nf}^{0.4}$ (experimental)	$Re_{nf} = 800 - 2.5 \times 10^3$ (laminar flow)	[30]
Water	Al_2O_3 TiO_2	3.16 vol%	Spherical	$Nu_{nf} = 0.021 \cdot Re_{nf}^{0.8} \cdot Pr_{nf}^{0.8}$ (experimental)	$\varphi \leq 3\% Re_{nf} = 10^4 - 10^5 Pr_{nf} = 6.54 - 12.33$	[18]
EG/W	Al_2O_3	10 vol%	Not available	$Nu_{nf} = 0.086 \cdot Re_{nf}^{0.55} \cdot Pr_{nf}^{0.5}$ (constant wall heat flux) $Nu_{nf} = 0.28 \cdot Re_{nf}^{0.35} \cdot Pr_{nf}^{0.36}$ (constant wall temperature)	$\varphi \leq 10\% Re_{nf} \leq 10^3 Pr_{nf} = 6 - 753$	[16,28]
Water	Cu	2.0 vol%	Spherical	$Nu_{nf} = 0.0059(1.0 + 7.628 \cdot \varphi^{0.6886} \cdot Pe^{0.001}) \cdot Re_{nf}^{0.9238} \cdot Pr_{nf}^{0.4}$ (experimental)	$Re_{nf} = 10^4 - 2.5 \times 10^4$ (turbulent flow)	[31]
Water	TiO_2	2.0 vol%	Spherical	$Nu_{nf} = 0.074 \cdot Re_{nf}^{0.707} \cdot Pr_{nf}^{0.385} \cdot \varphi^{0.074}$ (experimental)	$\varphi \leq 1\% Re_{nf} = 3 \times 10^4 - 1.8 \times 10^4$ (turbulent flow)	[32]
EG/W	TiO_2	0.02 vol%	Spherical	$Nu_{nf} = 0.007253 \cdot Re_{nf}^{0.8} \cdot Pr_{nf}^{0.5} \cdot (1 + \varphi)^{7.6}$ (experimental, no helical inserts)	$\varphi \leq 2\% Re_{nf} = 4 \times 10^3 - 1.5 \times 10^4$ (turbulent flow)	[33]

scaling laws for thermal conductivity and dynamic viscosity as functions of the base fluid properties, proposed by Corcione [25] which highlight that results from multiple experiments can be satisfactorily correlated, and in the benchmark projects in [26,27].

Those pending questions stand as foundations for the present study, where the most representative base fluid (i.e., EG/W) and the most stable nanofluid (i.e., TiO_2-EG/W) were employed to present an experimental and theoretical analysis, including a discussion on both laminar and turbulent flow regimes. As previously mentioned, they were selected to reduce the number of tested coolants, without penalizing the general applicability of the developed model. To support the theoretical assessment, an experimental apparatus to evaluate heat transfer with the base fluid and the nanofluid was designed and realized, and tests were conducted with a conventional coolant (i.e., 30%/70% ethylene glycol/water solution) and a TiO_2-based nanofluid with the same base fluid (TiO_2-EG/W solution). A fluid circuit with hot water served as the heat source in a liquid-liquid heat exchanger. Experiments were carried out for several flowrates in laminar regime and results are presented in terms of heat flowrate and required pumping power. As the theoretical contribution, the potential in using nanofluids is discussed through two independent FoM that are introduced and applied to both laminar and turbulent conditions. In the former flow regime, the experimental results are included to corroborate the validity of the presented relationships. The theoretical model provides a method to evaluate whether nanofluids are a promising choice or not at the design stage, thus progressing from the common *a posteriori* evaluation available in the current literature and filling a crucial gap in engineering. The study aims at supporting the design and implementation of nanofluids in cooling systems, by offering a method to generalize specific results and to critically assess the actual advantages from their use. Overall, an advancement in the use of nanofluids for cooling is provided, allowing to predict whether gain or drawback is yielded in terms of heat transfer rate and pumping power.

2. Experimental approach and procedure

2.1. Setup

An experimental apparatus was devised and developed to evaluate the performance of the tested coolants in terms of heat flowrate and required pumping power. The setup is shown in the photo of Fig. 1a, while a sketch is also presented in Fig. 1b. The test rig consisted of two separate hydraulic circuits, one for the hot fluid employed as the heat source and the other for the cold fluid (i.e., the coolant). The two lines featured 13 mm inner-diameter pipes; thermal interaction between the two circuits occurred in a liquid/liquid heat exchanger that was thermally insulated with three glass-wool layers (Acoustic 225 Plus by *Rockwool*), featuring thermal conductivity of 0.03 W m^{-1} K^{-1} and whole

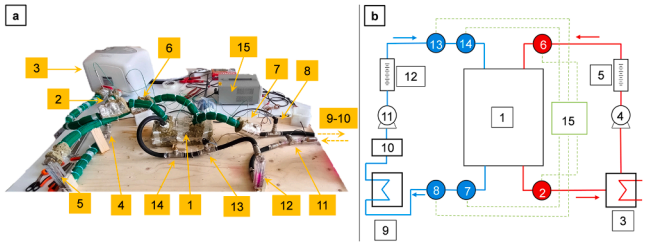

Fig. 1. Experimental setup: (a) photo of the test rig; (b) sketch of the cold/hot : (1) plate liquid/liquid heat exchanger, (2) thermocouple (hot fluid, inlet), (3) electric heater, (4) hot-fluid pump, (5) flow meter (hot fluid), (6) thermocouple (hot fluid, outlet), (7) thermocouple (coolant, outlet), (8) pressure transducer (coolant, outlet), (9) chiller, (10) reservoir for the coolant, (11) coolant pump, (12) flow meter (coolant), (13) pressure transducer (coolant, inlet), (14) thermocouple (coolant, inlet) and (15) data logger.

thickness of 90 mm, thus virtually eliminating heat dissipation to ambient air. Notably, the heat exchanger presented a 10-plate design with 45° chevron angle and 4 mm hydraulic diameter D_h for each channel. This length was calculated by the classic formula $D_h = 4\,A/p$, with A and p being the flow passage area and the wet perimeter, respectively; the actual cross-sectional surface is square, with 4 mm side length. The hot fluid (i.e., water) was heated by a 15 L electric heater with 3 kW maximum power. The maximum water temperature reached in all tests lay in the range of 60 - 65 °C, consistent with PEMFC operating temperature [3,4]. However, 5 °C fluctuations were observed by monitoring temperature throughout each test. Those oscillations were arguably due to the heater control system being operated on temperature feedback and inherently yielding to a delayed response. Moreover, a chiller was also included in the circuit to restore coolant temperature back at its initial value after exchanging heat with the hot fluid; that was achieved by making the coolant pass through a set of ice packs hosted in an insulated container. Each line was equipped with a flowmeter by *Key Instruments*, two K-type thermocouples (accuracy compliant with IEC 584 standard, class 1 tolerance) located in the proximity of the heat exchanger inlet/outlet sections (i.e., at 10 cm distance from them along the pipe). Notably, thermocouples were installed orthogonally to the pipe axis by using T-shaped junctions, with each thermocouple bead (i.e., the actual probe) being located onto the pipe axis to ensure a temperature measurement as far as possible from the thermal boundary layer over the sampling section. A centrifugal pump allowing a maximum flowrate of 10 L min^{-1}. The cold line was also equipped with two pressure transducers by *Gems Sensors* (3100 Series) to measure the pressure drop of the coolant through the heat exchanger, as they were placed right upstream of its inlet and downstream of its outlet, respectively. The sampling frequency was set as one acquisition per second for temperature and pressure measurements, respectively; on the other hand, flowrate was visually monitored over the flow meter scale. All readings were recorded using an 8-channel data logger by *Pico Technology* and analyzed by a self-developed MATLAB code. The layout and components of the test bench are included and listed in Fig. 1b. During each test, an initial transient phase was necessary to allow the system (i.e., both the operating fluids and the solid parts) to reach steady-state conditions. Notably, the derivative of the coolant temperature at heat-exchanger inlet was monitored as a marker to distinguish transient from steady state, with the dataset being analyzed only once that derivative became lower than 0.5 K min^{-1}, which was identified as a reasonable threshold. After such criterion was satisfied, typically requiring 5 - 6 min, data acquisition was carried out for 20 - 25 min. A slight variability in coolant temperature at the heat-exchanger inlet is inherently due to the finite volume of the chiller, which makes achieving constant temperature only asymptotical (i.e., the achieved steady-state condition is a practical approximation).

As mentioned in the introduction (Section 1), the tested coolants (cold line) are an ethylene glycol/water mixture (EG/W, 30% - 70% volume fraction) and a Ti-based nanofluid prepared by having the same coolant as the base fluid (i.e., 1 wt% TiO_2-EG/W nanofluid). The whole circuit was rinsed out after each test involving the prepared solution with nanofluids. Tests were carried out alternating the use of base fluid and nanofluid; the consistency of the acquired dataset (i.e., pressure loss, identified as the marker) indirectly proves the absence of relevant solid deposits onto the inner surface area of the plate heat exchanger and of the pipes.

2.2. Preparation and characterization of nanofluids

As mentioned in Section 2.1, titanium dioxide (TiO_2) nanoparticles were employed to prepare the nanofluid used in the present work; more specifically, anatase and rutile were purchased from *Sigma-Aldrich,* featuring minimum purity of 99.50%. The used powder generally exhibits poor water dispersibility and rapid flocculation upon exposure to aqueous media. Those nanoparticles present an average size of 20 nm,

as claimed by the manufacturer for the Degussa (Evonik) Aeroxide® P25 Titanium(IV) oxide (TiO_2) product, whose adoption is also reported in [37,38], which also features rutile/anatase ratio of 85:15 and 99.9% trace metals basis, as also reported in the INSCX™ Global Nanomaterials Exchange and Information Portal. According to the supplier, the nanoparticles exhibit an irregular faceted morphology, so their surface may present various shapes and angles, rather than being perfectly spherical. However, even though individual particles have an irregular morphology, the material as a whole consists of clusters or agglomerates of particles that are somewhat spherical, which suggests that those particles tend to form aggregates, arguably as a result of Van der Waals forces and interparticle interaction. An assessment of the specific surface area of the selected nanoparticles was carried out by the Accelerated Surface Area and Porosity System ASAP™ 2020 by *Micromeritics*, which implements the BET (Brunauer-Emmett-Teller) theory on both the supplied TiO_2 nanopowder (i.e., "as received" from the manufacturer) and the particles obtained from the dried suspension. The measurements revealed a specific surface area of 9.49 - 12.84 $m^2 g^{-1}$ for the latter, while the specific surface area of the former (i.e., their original solid state) resulted as equal to 50 $m^2 g^{-1}$, which is in agreement with findings reported in the available literature [39]. The significant reduction in the values of TiO_2 powder between the "as received" and the dried state can be attributed to the changes that occur during the drying process. In the former, powder might exhibit certain characteristics that contribute to a relatively higher value, which may include agglomeration or the presence of surface contaminants or adsorbed molecules. However, when the powder is subject to the drying process and forms dried powder, several changes may occur that lead to a significant reduction in the specific surface area, such as:

- during the drying process, nanoparticles are typically dispersed in a liquid medium; the drying process removes the liquid phase, leaving dried powders; this step can lead to increasing agglomeration.
- the drying process may lead to changes in the packing arrangement of nanoparticles; if that results in a more open and less dense structure, the surface area available for interaction increases, ultimately resulting in a lower value measured through BET theory.

As the tools to perform mixing between particles and base fluid (i.e., the EG/W mixture), both an ultrasonic stirrer (ultrasonic cleaning bath Transsonic Analog T460-H by *Elma*, with nominal frequency of 35 kHz) and a mechanical overhead stirrer (EUROSTAR 20 Digital Laboratory Overhead Stirrer by *IKA*, with speed range 0/30 - 2000 rpm) were used to actually carry out the whole process. Notably, as the first step to prepare the suspension, titania was dissolved in a mixture of water and ethylene glycol via ultrasonic stirring for 30 min in the presence of citric acid to fix pH at 6.5; that suspension was then agitated by mechanical stirring for the next 24 h. It is also worth mentioning that a surfactant (i.e., sodium tripolyphosphate) and a MEG/PEG (monoethylene/polyethylene glycol) mixture were added to the nanofluid towards reducing the attractive forces on the nanoparticles and stabilize their dispersion within the continuum. The same amount of both the surfactant and citric acid were kept constant over the whole prepared suspension. Sodium tripolyphosphate does not interact with the pH changer. When used in weak acidic media, it exhibits emulsifying and dispersing ability, thus effectively stabilizing emulsions and dispersing particles in the medium. Moreover, it can act as a chelating agent, binding to metal ions and preventing their adverse effects in a weak acidic environment. It also demonstrates wetting capability, facilitating the spreading and absorption of the surfactant onto solid surfaces. Citric acid was selected over HCl and HNO_3 for the performed experiments, thanks to its ability to optimize dispersion and stability of Ti-based nanoparticles in a mixture with water and water/organic solvents. It acts as a dispersing agent and surfactant by adsorbing onto the nanoparticle surface, thus forming a protective layer. This layer ultimately prevents agglomeration and aggregation of nanoparticles. Citric acid is effective in stabilizing nanoparticles mainly as a result of its negative charge. The carboxylate groups present in citric acid impart a negative charge, leading to electrostatic repulsion between nanoparticles. This repulsion hinders aggregation by generating a barrier between particles. Citric acid also exhibits chelating properties, which implies binding to metal impurities. This feature prevents interaction between impurities and nanoparticles, finally reducing aggregation. The chelating properties of citric acid allow maintaining stability of the dispersion: in addition to electrostatic and chelating effects, citric acid also promotes steric stabilization. The adsorbed citric acid molecules form a barrier between nanoparticles, thus reducing the attractive forces between them. This additional effect also contributes to prevent agglomeration and enhance dispersion.

The characterization of the EG/W-TiO_2 nanofluid consisted of measurements of electrokinetic potential (i.e., Zeta-potential), density, thermal conductivity, and dynamic viscosity. The average temperature of the base fluid when employed as the coolant, recorded by the thermocouples located at the inlet and outlet sections of the heat exchanger, were 30 and 50 °C, respectively. Therefore, nanofluid thermophysical properties were evaluated at 40 °C (i.e., the arithmetic mean of the two) and the results are summarized in Table 2. Notably, density was determined by measuring the ratio between liquid mass and volume in a graduated cylinder, which resulted in a 5% deviation from the value predicted theoretically by Eq. (1). Thermal conductivity measurements were conducted using the KD2 Pro-Thermal Properties Analyzer by *Decagon Devices*, which includes a manual controller and a sensor in contact with the fluid sample. The suspension was placed in a cylindrical specimen holder; six repeated measurements were conducted on each prepared sample, allowing a 15 min interval between measurements to make the liquid sample reach the thermal equilibrium. The measured values exhibited a 5% deviation from the prediction based on the model by Yu and Choi [22], which was then used as a reference for thermal conductivity of the nanofluid solution.

Zeta-potential measurements were conducted on the prepared nanofluid suspension by a Zetasizer Pro-instrument by *Malvern Panalytical*; those tests were carried out at 25 °C and with pH ranging from 4.61 to 10.51. As the substances used to vary pH, citric acid $C_6H_8O_7$ 0.1 M and an ammonium hydroxide solution at 0.001 M were added. The results of those measurements are presented in Table 3, which reveal the high degree of stability in the whole system, particularly as pH lies in the 6.13 - 8.56 range. The highest value (−53.5 mV) was recorded at pH 7.48, with the standard deviation being 6.1 mV. Granulometry was also performed employing a Mastersizer 2000 instrument by *Malvern Panalytical*. The investigated samples appeared as monodispersions, the size distribution of which featured a Gaussian-like curve (Fig. 2).

When considering the tests conducted at 25 °C room temperature and pH 6.8 as a representative example (Fig. 2), the average size (i.e., the harmonic-intensity-averaged particle diameter in accordance with standard ISO 13,321 for particles or molecules dispersed in a solution) resulted as 248 nm, as shown in Fig. 2; the distribution also showed a 111.1 nm average span. This aspect is relevant considering the monosized-particle nanofluids used by Yu and Choi [22] to develop their model, the applicability of which is nevertheless considered acceptable

Table 2
Thermophysical properties of the base fluid (EG/W, 30% - 70%) and nanofluid (EG/W- TiO_2) at 40 °C.

	Ethylene glycol-water (EG/W, 30%−70%)	TiO_2-EG/W nanofluid (Ti-NF)
Nanofluid volume fraction	–	1%
Density at 40 °C (kg m^{-3})	1044	1076
Thermal conductivity at 40 °C (W m^{-1} K^{-1})	0.4730	0.490
Specific heat at 40 °C (J kg^{-1} K^{-1})	3680	3650
Dynamic viscosity at 40 °C (Pa s)	1.57×10^{-3}	1.70×10^{-3}

Table 3
Zeta potential and average size of particles for nanofluid (TiO_2-EG/W) at 25 °C ambient temperature and at different sonication time.

pH-controlling substance	pH	Potential (mV)	Average size (nm)
$C_6H_8O_7$ 0.1 M	4.61	−35.7 ± 11.2	299.2
$C_6H_8O_7$ 0.1 M	4.87	−41.8 ± 8.8	315
$C_6H_8O_7$ 0.1 M	5.15	−42.7 ± 10.3	300.2
$C_6H_8O_7$ 0.1 M	5.48	−44.3 ± 9.4	302
$C_6H_8O_7$ 0.1 M	6.53	−50.8 ± 7.8	298.8
NH_4OH 0.001M	7.48	−53.5 ± 6.1	291.8
NH_4OH 0.001M	8.56	−51±11.3	304.7
NH_4OH 0.001M	9.08	−51.5 ± 10.2	302.9
NH_4OH 0.001M	9.78	−49.8 ± 11.4	295.4
NH_4OH 0.001M	10.51	−46.9 ± 9.8	292.4

to the solution used in the present work, even in the light of the previously mentioned comparison with measurements of thermal conductivity. The detected values fell into operating range of the instrument (0.02 - 2000 μm); average size is also reported in Table 3 for various pH values and combined with Zeta potential. In the solid discontinuous state (i.e., powder), the suspension samples exhibited particle size mostly larger than 20 nm (i.e., the average size claimed for the dry powder), which could be attributed to the formation of agglomerates during the dispersion phase within the liquid continuum. This explanation is supported by the relatively low Zeta-potential values (Table 3). Nevertheless, the size of such aggregates did not imply fast sedimentation and the suspension remained stable for extended periods of time (on the order of weeks), even when merely stored quiescent. An estimate of sedimentation velocity by Stokes' law yielded values smaller than 1×10^{-7} m s^{-1}, which emphasize the stability of those suspensions, supporting the choice of TiO_2-based suspensions in terms of stability. In fact, when TiO_2 nanoparticles are suspended, they tend to form clusters or agglomerates; nevertheless, the stability of the investigated suspensions is sufficiently robust to ensure effective performance as a coolant. As an additional test, pH 6.6 (in fact, maintained equal to 6.55 ± 0.18) was selected as representative: Zeta potential measurements and granulometry were performed on the prepared nanofluids were conducted at different sonication times imposed to the abovementioned ultrasonic cleaning bath. The outcomes of this analysis, also included in Tables 3 for different pH values and in Table 4 for sonication time at pH = 6.55 ± 0.18, suggest that a sonication time of 1 h appears optimal for the present experiments, since it provides effective dispersion of the TiO_2 particles in the solution by reducing their average size down to less than 300 nm, with this parameter not decreasing remarkably through longer sonication. Zeta-potential and pH measurements were taken on the nanofluid even after 15 runs of the experimental tests to check on potential performance loss of the employed surfactant. Actually, Zeta potential remained consistent, while pH slightly increased, arguably as a result of the partial dissolution of the surfactant in the investigated solutions. However, the suspension showed remarkable stability, since minimal or insignificant sedimentation of nanoparticles was detected.

As a significant thermophysical property, dynamic viscosity was also measured by a HAAKE RheoStress 100 rotational viscometer by *Thermo Scientific*. The analysis was conducted in control-rate mode with a 60 mm diameter flat-cone measuring sensor. The imposed shear rate was varied from 0 to 3000 s^{-1} and measurements were taken at 25 °C, although a decrease of dynamic viscosity with temperature is expected [40]. The results are presented in Fig. 3; notably, Fig. 3a shows the viscosity trend, while Fig. 3b shows the shear stress-to-rate relationship, confirming that the prepared nanofluid exhibits a Newtonian behavior. It is also worth noting that the experimental tests yielded values within ±7% span with respect to viscosity values predicted through the model by Wang et al. [32].

2.3. Experimental procedure and results

As a parametric analysis based on experimental results, three configurations were tested for each investigated coolant, which are summarized in Table 5. Notably, flowrate was varied within both the hot and the cold circuit, which led to a variation of the respective *Re*. The flowrate values were specifically selected to cover the entire range allowed by the developed experimental setup (i.e., the selected pump) and the results were then used as a dataset to substantiate the theoretical model, highlighted in the Introduction (Section 1) as the main objective of the present work. As recalled in Section 2.1, data acquisition for each test was started once the coolant-temperature derivative at the inlet of the heat exchanger became lower than 0.5 K min^{-1}, which makes the acquired dataset referred to steady-state conditions. Towards performing some statistical analysis, each test was repeated three times, since the developed experiment is typical of lab-scale research and very canonical, with very little sources of error other than those associated with measuring instruments. Regarding the coolant flow, its mean velocity

Table 4
Zeta potential and average size of particles for nanofluid (TiO_2-EG/W) at 25 °C ambient temperature and at different sonication time for pH = 6.55±0.18.

Sonication time (min)	Potential (mV)	Average size (nm)
0	−50.2 ± 7.8	678.5
30	−51.5 ± 6.5	372.7
60	−52.5 ± 7.1	268.1
120	−51.5 ± 6.0	263.1
180	−50.5 ± 6.1	251.9

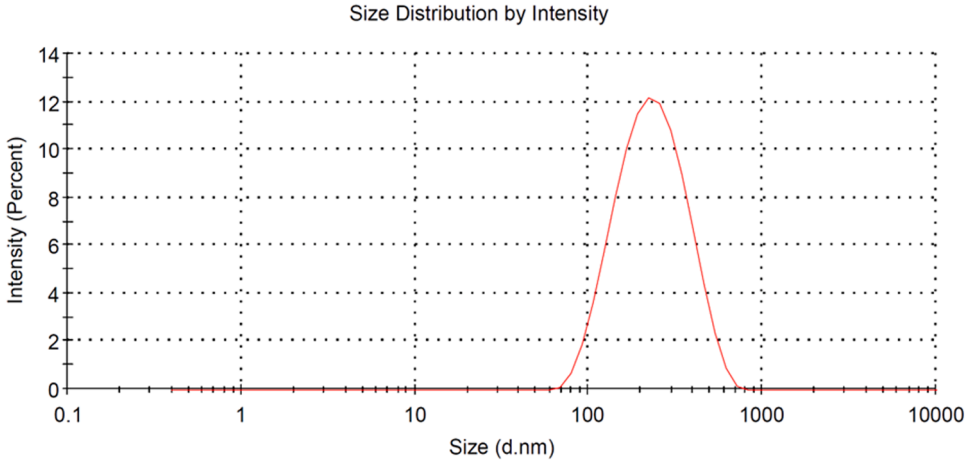

Fig. 2. Particle size distribution for the TiO_2-based nanofluid with pH 6.8 and at 25 °C room temperature.

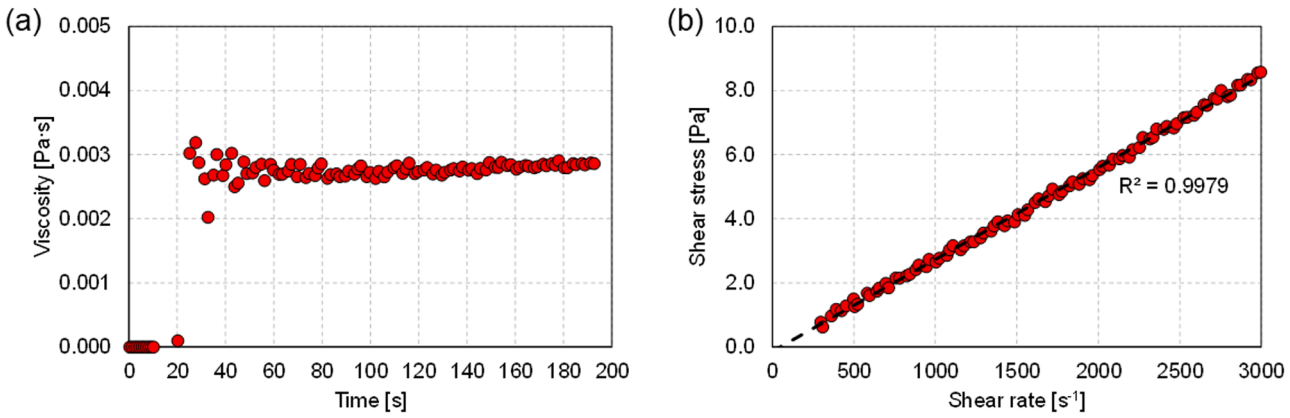

Fig. 3. Results from measurements of dynamic viscosity of the EG/W-TiO_2 nanofluid at 25 °C: (a) dynamic viscosity measured over a 200 s sampling time; (b) relationship between shear rate and shear stress.

Table 5
Flowrate evaluated Reynolds number and coefficient of variation for each tested configuration.

Test	L1	L2	L3
Hot-fluid flowrate (l min^{-1})	1.2	1.5	1.2
Coolant flowrate (l min^{-1})	2.8	3.0	2.0
Re	$\overline{Re}_{bf}$ = 327, $CoV_{Re_{bf}}$ = 2.3% $\overline{Re}_{nf}$ = 314, $CoV_{Re_{nf}}$ = 6.7%	$\overline{Re}_{bf}$ = 390, $CoV_{Re_{bf}}$ = 3.6% $\overline{Re}_{nf}$ = 360, $CoV_{Re_{nf}}$ = 6.1%	$\overline{Re}_{bf}$ = 241, $CoV_{Re_{bf}}$ = 11.0% $\overline{Re}_{nf}$ = 226, $CoV_{Re_{nf}}$ = 3.3%

within the plate heat exchanger channel was calculated by the following relationship:

$$v = \frac{\dot{V}}{A_{eff}}, \tag{3}$$

where $\dot{V}$ is the volumetric flowrate (measured by the flow meter) and A_{eff} is the effective cross-sectional area of the heat exchanger, which could be evaluated by considering the hydraulic diameter of each passage D_h (= 4 mm) and the number of parallel channels (= 5). The coolant velocity is hereafter referred to as v_{bf} and v_{nf} for the base fluid and the nanofluid, respectively. The Reynolds number *Re* was also calculated for the coolant in the channels of the heat-exchanger, as expressed by the following relationship:

$$Re = \frac{\rho v D_h}{\mu}. \tag{4}$$

The calculation employed density and dynamic viscosity of the base fluid and the nanofluid (ρ_{nf}, ρ_{bf}, μ_{nf}, μ_{bf}, respectively) to calculate Re_{bf} and Re_{nf}. This dimensionless quantity was assessed for each repeated test over all the investigated configurations, with the variation being due to the dependence on temperature of density and viscosity, whereas flowrate remained constant and equal to the values reported in Table 3. Notably, density and viscosity of the base fluids were taken from a recognized database [41], while the same properties for the nanofluid were calculated by Eqs. (1) and (5) [42], respectively. The dynamic viscosity increase expressed by Eq. (5) for 1% nanoparticle loading is μ_{nf}/μ_{bf} = 1.09, an estimate similar to that from other correlations for dynamic viscosity of nanofluids [43,44] (1.04 - 1.05).

$$\mu_{nf} = \mu_{bf} \cdot \left(1 + 7.3 \cdot \varphi + 123 \cdot \varphi^2\right). \tag{5}$$

The variation with respect to the mean value could be expressed by the Coefficient of Variation (CoV), which is the ratio between standard deviation and mean value (Table 3); the listed values support repeatability of the performed experiments. It is worth clarifying that those are estimates of *Re* at the inlet section of the heat exchanger, since the details of the design of its internal structure were unknown; the forced flow regime, driven by the circulating pump, at $Re > 200$ for all cases excluded the onset of Stokes flow. However, those values allowed identifying the flow regime, which was the actual scope, rather than a precise assessment of *Re* evolution through the heat exchanger. The available equipment limited the tested conditions to laminar flow regime for all the employed fluids. The experimental results are reported in Fig. 4 in terms of exchanged heat flowrate $\dot{Q}$, global heat transfer coefficient *U*, temperature difference and pressure drop of the coolant between inlet and outlet. The heating rate could be calculated by a simple power balance applied to the coolant as in Eq. (6), where the fluid mass flowrate and the mean fluid temperature at outlet and inlet sections ($\dot{m}$, T_{out} and T_{in}, respectively) were measured, while specific heat was calculated:

$$\dot{Q} = \dot{m} \cdot c \cdot (T_{out} - T_{in}). \tag{6}$$

Consequently, the global heat transfer coefficient could also be calculated as in Eq. (7) through the well-known Logarithmic Mean Temperature Difference applied to the involved heat exchanger, having the exchange area (A_{exh}) as a known parameter from the specifications made available by the manufacturer and all temperatures at inlet/outlet sections for both hot/cold fluid measured by thermocouples:

$$U = \frac{\dot{Q}}{A_{exh} \cdot \frac{\left(T_{h,in} - T_{c,out}\right) - \left(T_{h,out} - T_{c,in}\right)}{ln\left(T_{h,in} - T_{c,out}\right) - ln\left(T_{h,out} - T_{c,in}\right)}}, \tag{7}$$

where *exh* refers to the whole surface area through which heat transfer occurs, *h* refers to hot fluid and *c* refers to cold fluid.

Finally, temperature increase and pressure drop, here presented as its absolute value, between outlet and inlet of the heat exchanger were simply calculated from temperature and pressure readings for the coolant, once virtually steady-state conditions were reached. Statistical analysis was performed by assessing the mean value for each parameter, together with standard deviation, following classic formulations [45].

As expected, in all the tested configurations the use of TiO_2-EG/W nanofluid led to an increase in exchanged heat flowrate global heat transfer coefficient and temperature increase of the coolant. These aspects appear to consistently favor the nanofluid over the base fluid for cooling purposes; however, as also remarked in the introduction, they are accompanied with higher pressure loss across the heat exchanger (Fig. 4d), which on the other hand emphasizes the larger pumping power required to make nanofluids circulate. The case with the highest

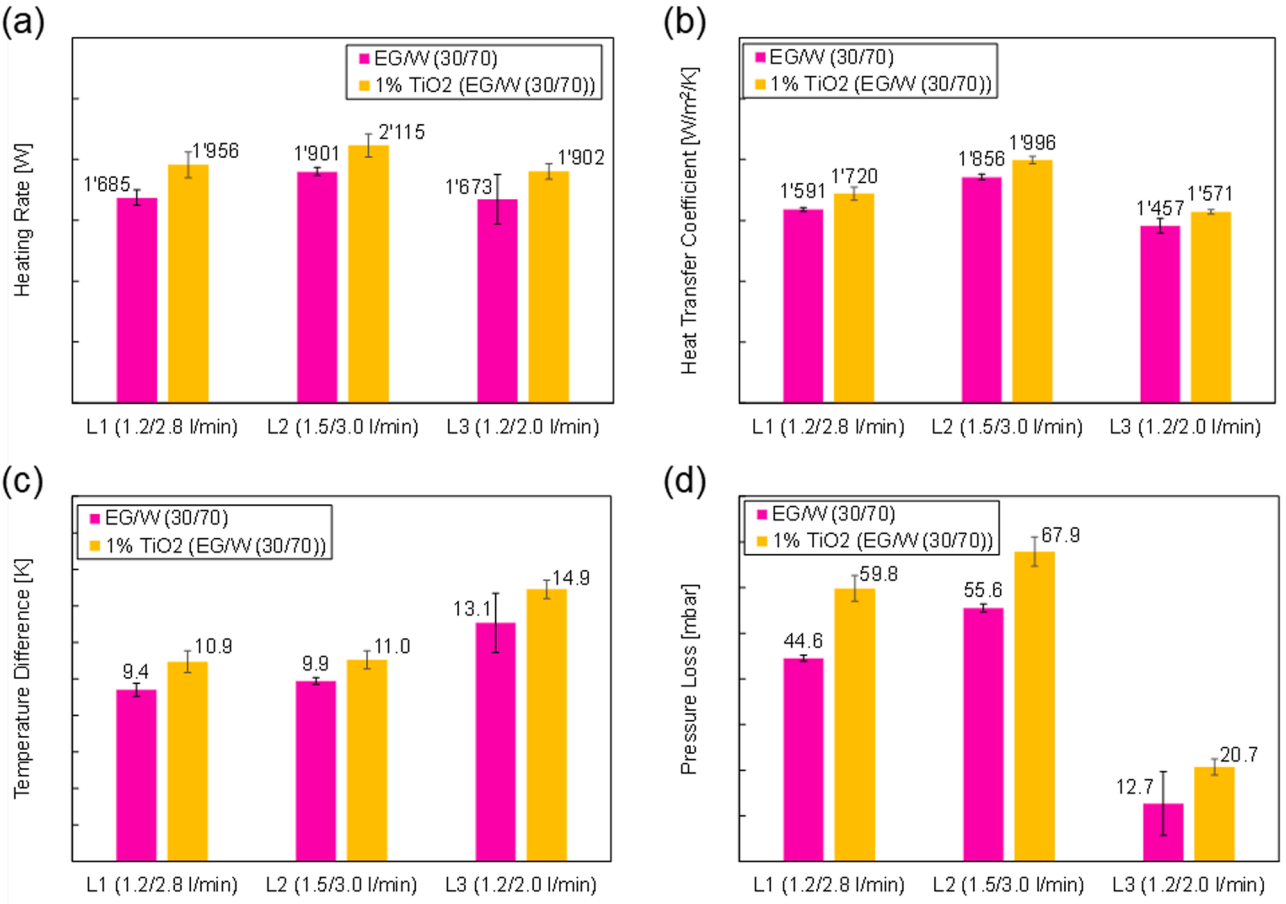

Fig. 4. Experimental results for EG/W and TiO_2-EG/W nanofluid, with mean value and standard deviation reported for each measured quantity: (a) exchanged heat flowrate, (b) global heat transfer coefficient, (c) temperature difference and (d) pressure drop of the coolant between inlet and outlet.

flowrate (L2) is also the one featuring the biggest exchanged heat rate, as also substantiated by the highest global heat transfer coefficient; this case also stands out as the one for which the highest pumping power was required. Case L3 is the one with the lowest coolant flowrate, hence showing the maximum temperature difference, due to the longest residence time of the coolant in the heat exchanger, and lowest pressure loss.

Those experimental outcomes confirm the general trend reported in the open literature of nanofluids and can be explained by the higher thermal conductivity, which implies higher heat flowrate, as well as bigger density and viscosity. Towards a generalized approach to the behavior of nanofluids, the obtained results served as an input to a physical model capable of distinguishing the various conditions and predict which of them yield an overall more effective action over conventional coolants.

3. Predictive modeling of nanofluids performance

A methodology is here proposed to provide guidance on: (i) whether the use of nanofluids is fully, partially or not beneficial to a given application under certain design conditions (e.g., flowrate, diameter) and, were it determined as beneficial, (ii) which characteristics the nanofluid flow should have. Notably, indications are provided through a combined analysis of heat transfer and parasitic power required for pumping, by independent Figures of Merit. The potential existence of conditions where gain on both aspects occurs (i.e., heat transfer increase and parasitic power reduction) is also discussed.

The presented method is based on two independent FoM for nanofluids: the comparison between nanofluid and employed base fluid in terms of heat transfer coefficient and parasitic pumping power. They are expressed by two nondimensional quantities: $h_r = h_{nf}/h_{bf}$ and $P_{p,r} = P_{p,nf}/P_{p,bf}$, quantifying the ratio between convective heat transfer coefficient h (h_{nf} and h_{bf}) and between pumping power P_p ($P_{p,nf}$ and $P_{p,bf}$), respectively. As expected, the best scenario for the use of nanofluids consists of $h_r \geq 1$ and $P_{p,r} \leq 1$, which results from $h_{nf} \geq h_{bf}$ and $P_{p,nf} \leq P_{p,nf}$; other less beneficial conditions are also possible. For each coolant (i.e., base fluid and nanofluid), the analysis was based on a specific model, derived from the characterization of the involved thermophysical properties (density ρ, specific heat c, dynamic viscosity μ and thermal conductivity k) and the evaluation of the involved dimensionless parameters (Re, Pr, Nu) by available correlations. The absence of undesired phenomena (e.g., sedimentation, agglomeration) is implicitly assumed; those mechanisms would challenge the applicability of any continuous flow model by generating large-scale solid regions and substantially modifying local momentum and heat transport. The model is presented in a generic form to make it of general validity and applicability, aiming at embodying an approach to carry out an *a priori* evaluation on nanofluids use, related to the associated flow conditions. Since the model is generic, it could be also applied to predict the performance of nanofluids prepared with non-spherical nanoparticles [9, 10], if and once their characterization in terms of thermophysical properties, stability and granulometry were available.

3.1. Figure of merit for convective heat transfer coefficient

The first FoM yields the already mentioned beneficial condition

($h_r \geq 1$; i.e., $h_{nf} \geq h_{bf}$), which could be expressed assuming the same circuit for the coolant ($D_{h,bf} = D_{h,nf}$; i.e., base fluid and nanofluid flow within the same channels and components). Therefore, the general definition $Nu = \frac{h \cdot D_h}{k}$ leads to the following condition:

$$Nu_{nf}\ k_{nf} \geq Nu_{bf}\ k_{bf}. \tag{8}$$

The general formulation for the Nusselt number is here presented for both the base fluid in Eq. (9) and for the nanofluid in Eq. (10), with the dimensionless Reynolds (Re_{bf}, Re_{nf}) and Prandtl numbers (Pr_{bf}, Pr_{nf}) being calculated for each fluid. As shown in Table 1, such generic formulations represent the numerous relationships available in the open literature. It is worth clarifying that Eqs. (9) and (10) serve as mere general expression, then adapted to the base fluid and nanofluid involved by suitable values for a_{bf}, b_{bf}, c_{bf}, a_{nf}, b_{nf}, c_{nf} coefficients.

$$Nu_{bf} = a_{bf}\ Re_{bf}^{b_{bf}}\ Pr_{bf}^{c_{bf}}, \tag{9}$$

$$Nu_{nf} = a_{nf}\ Re_{nf}^{b_{nf}}\ Pr_{nf}^{c_{nf}}. \tag{10}$$

The mean velocity of each fluid (v_{bf} and v_{nf}) is included in the Reynolds numbers and expressed by the relationship of Eq. (4). Introducing Eqs. (9) and (10) in Eq. (8) and elaborating it as function of the respective fluid velocities (v_{bf} and v_{nf}), the following condition for v_{nf} can be obtained:

$$v_{nf} \geq \sqrt[b_{nf}]{v_{bf}^{b_{bf}} \frac{a_{bf}}{a_{nf}} \frac{\rho_{bf}^{b_{bf}}}{\rho_{nf}^{b_{nf}}} D_h^{(b_{bf}-b_{nf})} \frac{\mu_{bf}^{(c_{bf}-b_{bf})}}{\mu_{nf}^{(c_{nf}-b_{nf})}} \frac{c_{p,bf}^{c_{bf}}}{c_{p,nf}^{c_{nf}}} \frac{k_{nf}^{(1-c_{bf})}}{k_{bf}^{(1-c_{nf})}}}. \tag{11}$$

Eq. (11) expresses the velocity condition for the nanofluid to attain an equal or higher heat transfer coefficient than the base fluid ($h_r \geq 1$), hence it provides a quantitative indication for the nanofluid flowrate through Eq. (3) towards augmenting heat transfer. However, this relationship does not contain any information on the associated pressure loss and parasitic power required for pumping; practically, it does not depend on circuit length or local losses, with only the channel diameter D_h being considered.

3.2. Figure of merit for pumping power

The second FoM identifies the flow conditions yielding an equal or lower pumping pressure required by the nanofluid with respect to the base fluid ($P_{p,r} \leq 1$; i.e., $P_{p,nf} \leq P_{p,bf}$). For a generic centrifugal pump, the power transferred to the fluid for pumping is given by $P_p = \Delta p \cdot \dot{V}$, with $\dot{V} = v \cdot A_{eff}$ by Eq. (3) and where Dp is the global pressure drop. Considering the same circuit for both the base fluid and the nanofluid, hence the same A_{eff}, a comparison in terms of pumping power flux $\left(p_p = \frac{P_p}{A_{eff}}\right)$ could be made, which yielded $p_p = \Delta p \cdot v$. A lower pumping power flux for the nanofluid corresponds to $p_{p,r} \leq 1$, with $p_{p,r} = p_{p,nf}/p_{p,bf}$.

The pressure losses are commonly grouped as friction (or major) losses and local losses, the former type being associated to skin friction of viscous flows, whereas the latter are due to sudden changes in the geometry (e.g., bends, junctions). The general relationship valid for both laminar and turbulent flows is reported in Eq. (12) [46], with f being the Darcy friction factor (equal to $\frac{64}{Re}$ for a fully developed laminar flow in a circular tube), and K_L being an equivalent local loss coefficient including all the pressure losses of this type.

$$\Delta p = \left(f\ \frac{L}{D_h} + K_L\right)\ \rho\ \frac{v^2}{2}. \tag{12}$$

The major and local loss coefficients were grouped for the base fluid and the nanofluid to preserve generality and referred to as $\chi_{bf} = f_{bf}\ \frac{L}{D_h} + K_{L,bf}$ and $\chi_{nf} = f_{nf}\ \frac{L}{D_h} + K_{L,nf}$, respectively, with L being the total extent of the pipes with the same hydraulic diameter. The general form of the inequality for pumping power flux is expressed by Eqs. (13) and (14), finally leading to the velocity condition for the nanofluid reported in Eq. (15):

$$\Delta p_{nf}\ v_{nf} \leq \Delta p_{bf}\ v_{bf}, \tag{13}$$

$$\chi_{bf}\ \rho_{nf}\ \frac{v_{nf}^2}{2}\ v_{nf} \leq \chi_{nf}\ \rho_{bf}\ \frac{v_{bf}^2}{2}\ v_{bf}, \tag{14}$$

$$v_{nf} \leq v_{bf} \sqrt[3]{\frac{\rho_{bf}}{\rho_{nf}}\ \frac{\chi_{bf}}{\chi_{nf}}}. \tag{15}$$

This embodies the velocity condition for the nanofluid to require a lower or equal pumping power flux than the base fluid ($p_{p,nf} \leq p_{p,bf}$), hence it provides an indication about the flowrate that makes the use of nanofluids reduce parasitic power. As opposed to the condition expressed about the first FoM (Section 3.1), it carries no information about heat transfer.

3.3. Flow regimes and performance evaluation

Based on the two independent FoM proposed, four possible scenarios arise. Each of them is associated to flow conditions (e.g., velocity, Reynolds number) specific to the considered configuration. The existence - if any - and the extent of each scenario depends on the fluid and flow regime involved. The scenarios are:

1. $h_{nf} \geq h_{bf}$, $p_{p,nf} \leq p_{p,bf}$: the most favorable, as the nanofluid presents both a higher heat transfer rate and a reduced parasitic power required with respect to the base fluid. In this scenario, using nanofluids is beneficial for both aspects.
2. $h_{nf} \geq h_{bf}$, $p_{p,nf} > p_{p,bf}$: in this scenario, the use of nanofluids increases heat transfer rate with respect to the base fluid, but at the cost of higher pumping power. The choice may be based on an application-specific assessment of gains and drawbacks and no general conclusions can be drawn.
3. $h_{nf} < h_{bf}$, $p_{p,nf} \leq p_{p,bf}$: nanofluids present a lower heat transfer coefficient, hence a reduced heat transfer rate, but also require lower parasitic power than the base fluid. The choice may be made on a case-by-case basis, as for the previous scenario.
4. $h_{nf} < h_{bf}$, $p_{p,nf} > p_{p,bf}$: the worst-case scenario, since the use of nanofluids yields both a lower hear transfer rate and a higher pumping power than those associated with the base fluid. In this scenario, the use of nanofluids is not recommended.

As an example, the previously described approach was applied to the fluids and setup employed in the experiments presented in Section 2: the base fluid was a 30%/70% EG/W mixture and the nanofluid was TiO_2-EG/W ($\varphi = 0.01$). However, the applicability of the proposed methodology is - in principle - general, so the approach can be employed to evaluate the performance of any other combination of base fluid and nanoparticle dispersion, only requiring fluid-specific characterization for both of them. In consistency with the performed experiments, the model assumes that stability is achieved for the nanofluid suspension, with failed stabilization or eventual long-term sedimentation lying out of its scopes. Regarding density and specific heat of the nanofluid, Eqs. (1) and (2) were used. Thermal conductivity was modelled by a recognized correlation [22], the applicability of which is also supported by the results proposed in Section 2.2, reported in Eq. (16), with $\beta = 0.1$ representing the ratio of the nanolayer thickness to the particle radius. Dynamic viscosity was calculated using Eq. (5), the predictive capability of which is also discussed in Section 2.2. The base fluid and nanofluid thermo-physical properties are shown in Fig. 5 as a function of the particle loading.

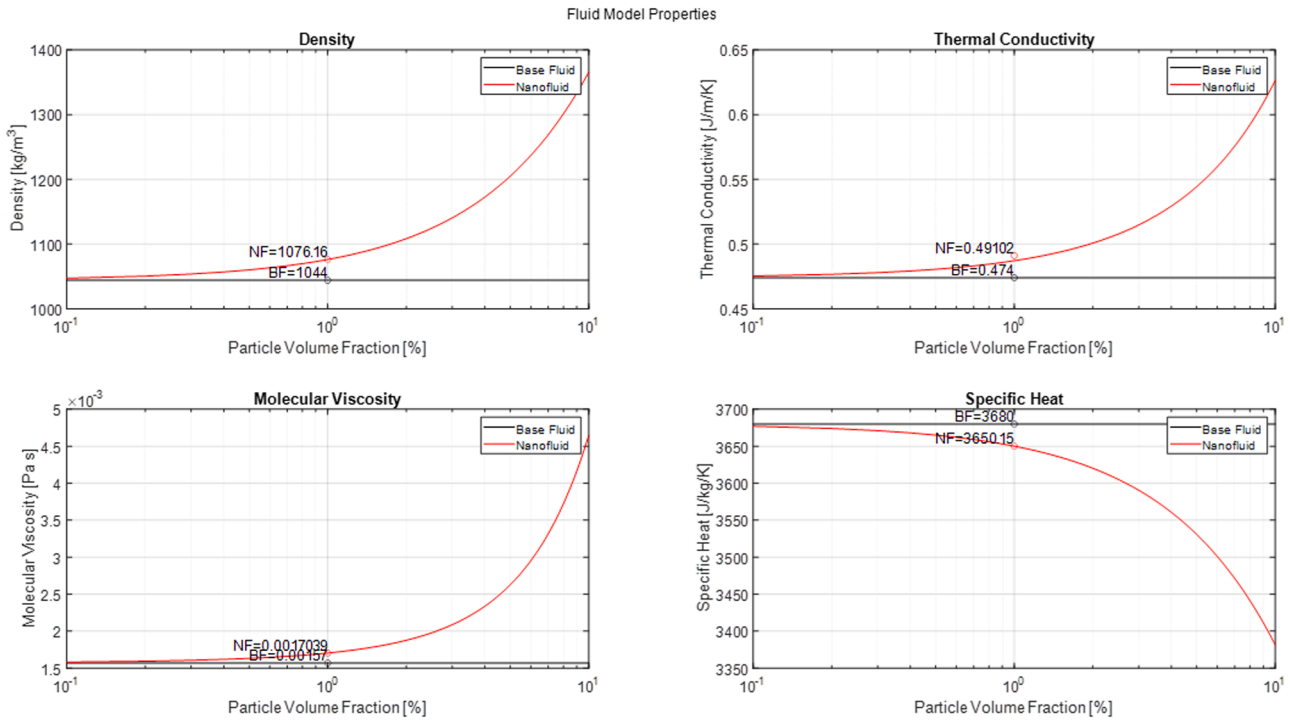

Fig. 5. Thermophysical properties for base fluid (30%/70% EG/W mixture) and nanofluid (TiO_2-EG/W) for increasing particle loading.

$$k_{nf} = \left[\frac{k_p + 2k_{bf} + 2\left(k_p - k_{bf}\right)(1+\beta)^3\varphi}{k_p + 2k_{bf} - \left(k_p - k_{bf}\right)(1+\beta)^3\varphi}\right] k_{bf}. \tag{16}$$

Regarding laminar flow regime, for the base fluid the $Nu_{bf} = 4.36$ [46] relationship was applied under the hypotheses of fully developed laminar flow in a circular channel, with constant heat flux. That results from the generic formulation of Eq. (9), by imposing $a_{bf} = 4.36$, $b_{bf} = 0$ and $c_{bf} = 0$. For the nanofluid, the experimentally derived correlation for fully developed laminar flow [30] was used, as also in Eq. (17) (Table 1). The friction factors for the laminar flow regime were experimentally expressed by Li and Xuan [30] as $f_{bf} = \frac{64}{Re_{bf}}$ and $f_{nf} = \frac{64}{Re_{nf}}$, respectively. Nusselt number and friction factor for the laminar case are presented in Fig. 6 as a function of the Reynolds number. It is evident that the selected correlations yield higher heat transfer rate for the nanofluid (i.e., $Nu_{nf} \geq Nu_{bf}$), if Reynolds number is bigger than 50. Notably, Nusselt number of the nanofluid could be calculated through the generic relationship of Eq. (10), by imposing $a_{nf} = 0.4328(1.0 + 11.285\ \varphi^{0.754}\ Pe_{nf}^{0.218})$, $b_{nf} = 0.333$ and $c_{nf} = 0.4$. The Péclet number of the nanofluid (Pe_{nf}) is defined as $Pe_{nf} = v_{nf} \cdot d_p / \alpha_{nf}$, with d_p and α_{nf} being the nanoparticle diameter and thermal diffusivity [30], respectively.

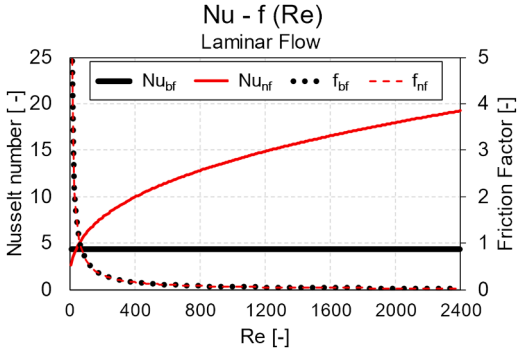

Fig. 6. Nusselt number (left y axis) and friction factor (right y axis) as a function of Re in laminar flow regime.

$$Nu_{nf} = 0.4328\left(1.0 + 11.285\ \varphi^{0.754}\ Pe_{nf}^{0.218}\right) Re_{nf}^{0.333}\ Pr_{nf}^{0.4}. \tag{17}$$

The analysis of the pumping power required for coolant circulation implied knowing the specific characteristics of the hydraulic circuit. In the present experiments, the extent of interest is the one enclosed between the inlet and the outlet sections of the heat exchanger, hence quantifying of the major and local pressure losses in this trait was demanded. Regarding the former, the hydraulic diameter (D_h) and channel length ($L = 0.1718\ m$) for each of the five passages was used, whereas an equivalent loss coefficient for the local losses was calculated as based on pressure-drop measurements. This embodied all the pressure losses resulting from the flow within the heat exchanger inner channels; an average value for the base fluid ($\overline{K_{Lbf}} = 597.7$, with standard deviation $\sigma_{K_{L,bf}} = 200.2$) and the nanofluid ($\overline{K_{Lnf}} = 787.3$, with standard deviation $\sigma_{K_{L,nf}} = 148.8$) were finally obtained. This aspect is specific to the employed circuit design, although this approach to evaluate pressure losses applies to any hydraulic circuit.

The results shown in Fig. 7 highlight that a region exists, which univocally supports the use of nanofluids in laminar flow regime (i.e., Case 1: $h_{nf} \geq h_{bf}, p_{p,nf} \leq p_{p,bf}$). This corresponds to the area above the red line ($h_{nf} \geq h_{bf}$; i.e., the first FoM) and below the blue line ($p_{p,nf} \leq p_{p,bf}$; i.e., the second FoM). In the laminar flow regime, the condition for the combined gain from using nanofluids is then present, remarkably indicating a preferential flow condition for their use for cooling purposes. At such flow regime, the combined gain in heat transfer and reduction of pumping cost are simultaneously achieved. This information provides an indication not only for the general use of nanofluids in the laminar flow regime, but also about the flow conditions to impose towards a combined gain in heat transfer and parasitic power. As shown in Fig. 7, such region is generally located below the line inclined at 45° in all plots; so, in the range $v_{nf} < v_{bf}$ and $Re_{nf} < Re_{bf}$, heat transfer augmented by nanofluids is present. The experimental data from L1, L2 and L3 tests in laminar flow regime - the only one feasible through the experimental setup (Section 2.3) - are added to Fig. 7, as well as the condition for equal pumping power flux ($p_{p,nf} = p_{p,bf}$). All tests show that under the same mean velocity ($v_{nf} = v_{bf}$, presented in Fig. 7a along the line inclined at

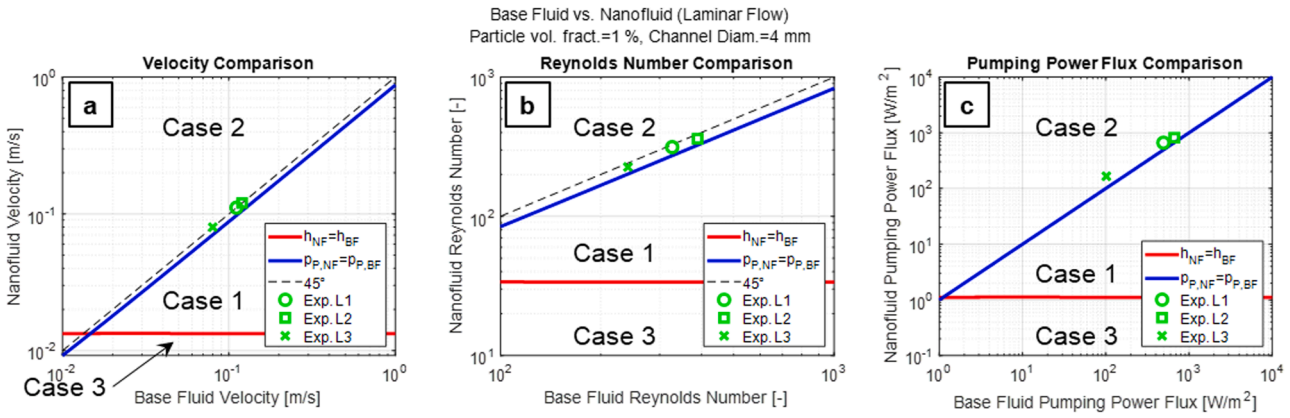

Fig. 7. Comparison between base fluid and nanofluids, and experimental datapoints (L1, L2, L3 from Table 5) for base fluid (x axis) and nanofluid (y axis) in terms of: (a) velocity, (b) Reynolds number and (c) pumping power flux for laminar flow regime.

45°), nanofluids feature $Re_{nf} < Re_{bf}$ (Fig. 7b, below the line inclined at 45°), due to the dominant effect of higher viscosity. The theoretical model also reveals that the tested L1, L2 and L3 conditions are close to the border - almost at the edge - with the Case 1 region, which allows inferring that pumping power could be reduced with respect to cooling by the base fluid through a reduction of nanofluid velocity, still benefiting from augmented heat transfer. This observation contextualizes the set of experiments within the proposed approach to the quantitative evaluation of nanofluid performance, while also providing a guidance to future experiments. However, Fig. 7c shows that all the tested conditions lie above the line identifying the same required pumping power flux; so, more power flux was needed for nanofluid circulation than that for base fluid in the performed experiments.

Regarding the theoretical distinction based on the two FoM, all the three tested conditions lie in the region where the analysis predicted higher heat transfer rate ($h_{nf} \geq h_{bf}$), which is also supported by the related measurements reported in Figs. 4a-c. As for pumping power flux, all the three acquisitions exhibit a higher pumping power flux for nanofluids (Fig. 4d), hence confirming the location of those datapoints in the Case 2 scenario ($h_{nf} \geq h_{bf}$, $p_{p,nf} > p_{p,bf}$). As an additional note, the here proposed model does not include Stokes flow, since Reynolds number is assumed as far higher than 1, even in applications where laminar flow regime occurs. However, the employed approach does not prevent its future inclusion.

An analogous approach was followed to compare nanofluids against base fluid in terms of heat transfer rate and required parasitic power under turbulent flow regime. The average heat transfer coefficient for the base fluid was calculated through the Dittus-Boelter correlation for Nu, as in Eq. (18) [46], whereas the convective heat transfer coefficient for the turbulent flow of TiO_2-EG/W nanofluid was derived from the regression analysis proposed by Duangthongsuk and Wongwises [32] for Nu_{nf}, as in Eq. (19):

$$Nu_{bf} = 0.023\ Re_{bf}^{0.8}\ Pr_{bf}^{0.4}, \tag{18}$$

$$Nu_{nf} = 0.074\ Re_{nf}^{0.707}\ Pr_{nf}^{0.385}\ \varphi^{0.074}. \tag{19}$$

The friction factor used to estimate major pressure losses for the base fluid was calculated using the Petukhov equation [46], as in Eq. (20), whereas the friction factor for the TiO_2-EG/W nanofluid was experimentally derived [32] and is expressed by Eq. (21). The local pressure loss coefficient was extrapolated for turbulent flows from the regression analysis presented in the previous part for the employed hydraulic circuit. Nusselt number and friction factor for both fluids in turbulent conditions are presented in Fig. 8 as a function of Reynolds number.

$$f_{bf} = \left[0.790\ ln\left(Re_{bf}\right) - 1.64\right]^{-2}, \tag{20}$$

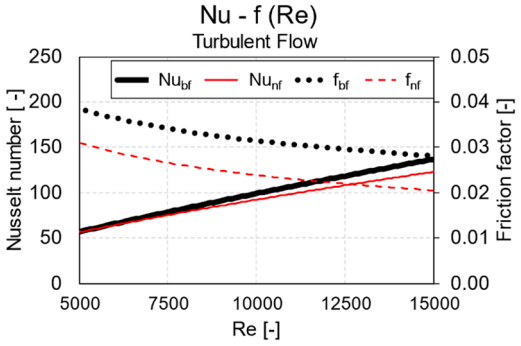

Fig. 8. Nusselt number (left y axis) and friction factor (right y axis) as a function of Re in turbulent flow regime.

$$f_{nf} = 0.3250\ Re_{nf}^{-0.2377}\ (1+\varphi)^{2.723}. \tag{21}$$

The results reported in Fig. 9 outline a different scenario than that observed for laminar flow conditions: the region where heat transfer gain occurs ($h_{nf} \geq h_{bf}$; i.e., above the red line) is separated from the region of pumping power flux gain ($p_{p,nf} \leq p_{p,bf}$; i.e., below the blue line), with no overlap. This observation yields that there is no possible flow condition where the use of this nanofluid is simultaneously beneficial in terms of both figures of merit: Case 1 scenario highlighted for laminar flow regime does not exist under turbulent flow regime. Therefore, a choice may be made between a nanofluid flow with higher heat transfer rate at the cost of increasing pumping power), or with reduced pumping power at the cost of lower heat transfer rate. These results provide a quantitative indication that advocates against the use of nanofluids for cooling applications where a turbulent flow regime is present, which can be a valuable information at the design stage. It is worth clarifying that the inherent limitations of the developed experimental apparatus prevented from running tests under turbulent conditions, hence no experimental data could be included in Fig. 9. The presented FoM and the arisen indications were combined and are presented in a single graph with non-dimensional parameters: the ratio between pumping power flux required by nanofluid and base fluid ($p_{p,nf}/p_{p,bf}$), and the ratio between the product of Nusselt number and thermal conductivity of nanofluid and base fluid ($Nu_{nf}\ k_{nf}$)/($Nu_{bf}\ k_{bf}$). Fig. 10 shows the four regions (i.e., the four scenarios) for the laminar flow regime, highlighting where the use of nanofluids appears beneficial (i.e., Case 1 scenario), as well as the tested conditions.

As previously mentioned, no Case 1 scenario would appear in a plot developed for turbulent flow conditions. Moreover, the quantitative analysis was performed against the circuit employed for the

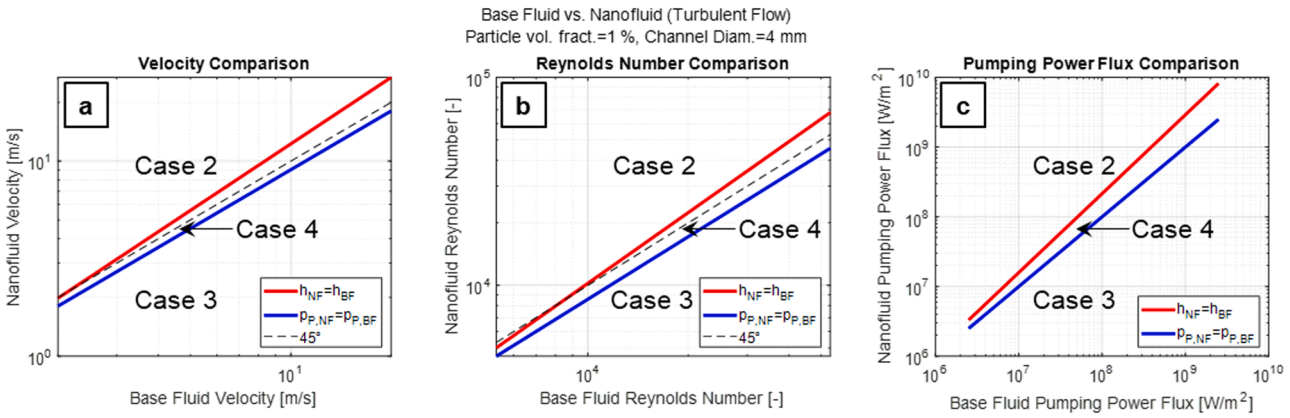

Fig. 9. Comparison between base fluid and nanofluids for base fluid (x axis) and nanofluid (y axis) in terms of: (a) velocity, (b) Reynolds number and (c) pumping power flux for turbulent flow regime.

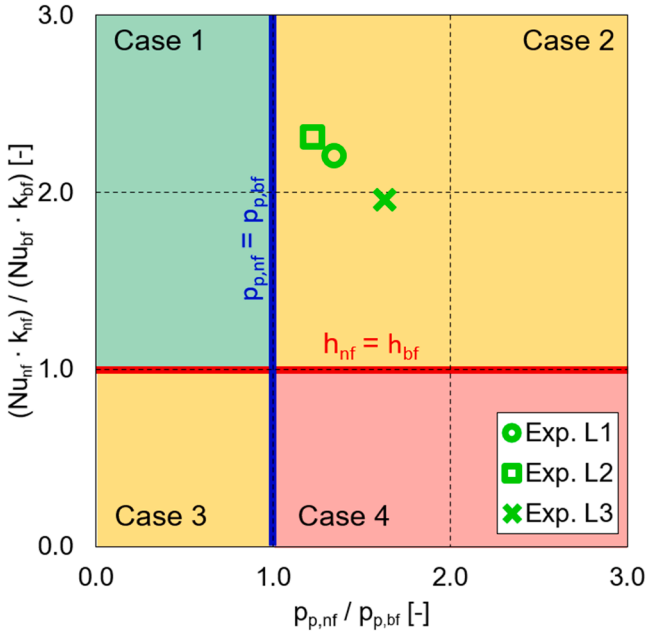

Fig. 10. Ratio of the product of Nusselt number and thermal conductivity between nanofluid and base fluid vs. ratio of pumping power flux between nanofluid and base fluid; the isolines identifying the same heat transfer coefficient and pumping power flux appear in red and blue, respectively.

experiments; however, the conditions expressed in Sections 3.1 and 3.2 are generic, so the approach may be applied to any specific configuration.

4. Conclusions

The present research is motivated by the quest for increasing heat transfer rate for cooling purposes, especially when the need for dissipating a large amount of heat is combined with space constraints (e.g., fuels cells employed in the automotive sector). Nanofluids have been known for decades as promising candidates to substitute conventional coolants, thanks to their augmented thermal conductivity and to the possibility to adjust solid nanoparticle concentration within the base fluid to meet the requirements of each specific application. However, the benefit from including nanoparticles should be put in the context of system design, which may also consider an increase in the required pumping power as a parameter of interest to assess the balance between heat removal and energy consumption.

To this end, both dedicated experiments and a theoretical model predictive of heat transfer and pressure drop are proposed to quantitatively discuss the conditions of actual improvement by using nanofluids with respect to conventional coolants. An experiment was devised and developed to compare a representative example of the latter (i.e., an ethylene glycol/water mixture) with a TiO_2-based nanofluid prepared by having it as the base fluid (i.e., TiO_2-EG/W, with 1% particle loading); the measured parameters allowed assessing both heat transfer rate and pressure loss in the circuit for various flowrate conditions. The employed nanofluid was also characterized in terms of the thermophysical properties involved. The experiments substantiated the enhanced heat transfer rate achieved by using nanofluids, which was, however, accompanied by higher pressure losses. The experimental dataset was then brought into the broader frame of a predictive physical model, aimed at assessing which conditions, if any, lead to an advantage in using nanofluids, by using two independent figures of merit, aiming at evaluating the potential simultaneous increase in heat transfer rate and decrease in parasitic power. The model showed that the conditions of combined gain exist in laminar flow regime, as a result of the higher Nusselt number for nanofluids. The $Nu_{nf} \geq Nu_{bf}$ condition also attained as Reynolds number increases moderately at values higher than 40, with the friction coefficient remaining comparable to that of the base fluid. Conversely, in turbulent flow regime, the combined condition of augmented heat transfer rate and reduced pumping pressure are not present, which is consistent with the common perception on nanofluids.

The present study shows that an *a priori* evaluation of the benefit from using nanofluids for cooling purposes is quantitatively feasible, as based on independent non-dimensional parameters (i.e., the figures of merit) that allow an approach predictive of the conditions of potential gain (or loss) with respective to conventional coolants. The proposed methodology may serve as a guidance of general validity for the design of cooling systems that employ nanofluids and it recommends their use in applications where cooling under laminar flow regime is can be implemented. As a hint to future developments, the inclusion of molecular thermodynamics may open potentially disruptive routes to modeling of nanofluids, also impacting on predictive approaches of their performance, as well as a rigorous evaluation of different base fluids and suspended particles is believed to provide preferential formulations, resulting in few candidate nanofluids for cooling engineering.

CRediT authorship contribution statement

Alessandro d'Adamo: Conceptualization, Methodology, Formal analysis, Investigation, Writing – original draft, Supervision, Funding acquisition, Project administration. **Martino Diana:** Software, Formal analysis, Investigation, Writing – review & editing. **Giuseppe Corda:** Software, Formal analysis, Investigation, Writing – review & editing.

Antonio Cucurachi: Software, Formal analysis, Investigation, Writing – review & editing. **Maria Cannio:** Formal analysis, Data curation, Writing – review & editing. **Andrea Pellacani:** Formal analysis, Investigation, Validation. **Marcello Romagnoli:** Formal analysis, Validation, Writing – review & editing. **Enrico Stalio:** Methodology, Validation, Writing – review & editing. **Paolo E. Santangelo:** Conceptualization, Methodology, Formal analysis, Investigation, Writing – original draft, Writing – review & editing, Supervision, Funding acquisition.

Declaration of Competing Interest

The authors declare the following financial interests/personal relationships which may be considered as potential competing interests:

Alessandro d'Adamo reports financial support was provided by University of Modena and Reggio Emilia. Alessandro d'Adamo reports a relationship with University of Modena and Reggio Emilia that includes: employment and funding grants.

Data availability

Data will be made available on request.

Acknowledgements

This research was supported by Università degli Studi di Modena e Reggio Emilia (Italy) through the FAR (Fondo di Ateneo per la Ricerca) Mission Oriented 2021 grant "NANO4COOL-NANOfluids For COOLing of PEM Fuel Cell Systems", funded by Fondazione Cassa di Risparmio di Modena (CUP: E95F21002900007). The authors wish to thank Dr. Veronica Testa for the invaluable suggestions and help through the characterization of the employed nanofluids.

References

[1] S.U.S. Choi, J.A. Eastman, Enhancing thermal conductivity of fluids with nanoparticles, Nano Energy 2 (5) (1995) 845–855, https://doi.org/10.1016/J.NANOEN.2013.02.007. Oct.

[2] S.K. Das, 'Nanofluids—the cooling medium of the future', vol. 27, no. 10, pp. 1–2, Dec. 2007, doi:10.1080/01457630600904585.

[3] I. Zakaria, et al., Experimental investigation of Al_2O_3 - water ethylene glycol mixture nanofluid thermal behaviour in a single cooling plate for PEM fuel cell application, Energy Procedia 79 (2015) 252–258, https://doi.org/10.1016/J.EGYPRO.2015.11.474. Nov.

[4] I. Zakaria, et al., Thermal analysis of Al2O3-water ethylene glycol mixture nanofluid for single PEM fuel cell cooling plate: an experimental study, Int. J. Hydrogen Energy 41 (9) (2016) 5096–5112, https://doi.org/10.1016/J.IJHYDENE.2016.01.041. Mar.

[5] I. Zakaria, W.A.N.W. Mohamed, W.H. Azmi, A.M.I. Mamat, R. Mamat, W.R. W. Daud, Thermo-electrical performance of PEM fuel cell using Al2O3 nanofluids, Int. J. Heat Mass Transf. 119 (2018) 460–471, https://doi.org/10.1016/J.IJHEATMASSTRANSFER.2017.11.137. Apr.

[6] N.A.C. Sidik, M.N.A.W.M. Yazid, R. Mamat, A review on the application of nanofluids in vehicle engine cooling system, Int. Commun. Heat Mass Transf. 68 (2015) 85–90, https://doi.org/10.1016/J.ICHEATMASSTRANSFER.2015.08.017. Nov.

[7] K. Elsaid, A.G. Olabi, T. Wilberforce, M.A. Abdelkareem, E.T. Sayed, Environmental impacts of nanofluids: a review, Sci. Total Environ. 763 (2021), 144202, https://doi.org/10.1016/J.SCITOTENV.2020.144202. Apr.

[8] A. Hajatzadeh Pordanjani, S. Aghakhani, M. Afrand, B. Mahmoudi, O. Mahian, S. Wongwises, An updated review on application of nanofluids in heat exchangers for saving energy, Energy Convers. Manag. 198 (2019), 111886, https://doi.org/10.1016/J.ENCONMAN.2019.111886. Oct.

[9] M. Ramzan, N. Shahmir, H.A.S. Ghazwani, K.S. Nisar, F.M. Alharbi, I.S. Yahia, Hydrodynamic and heat transfer analysis of dissimilar shaped nanoparticles-based hybrid nanofluids in a rotating frame with convective boundary condition, Sci Rep 12 (1) (2022) 1–17, https://doi.org/10.1038/s41598-021-04173-z. *2022 12:1*Jan.

[10] X. Li, et al., Heat transfer enhancement of nanofluids with non-spherical nanoparticles: a review, Appl. Sci. 2022 12 (9) (2022) 4767, https://doi.org/10.3390/APP12094767. *Vol. 12, Page 4767*May.

[11] B. Mehta, D. Subhedar, H. Panchal, Z. Said, Synthesis, stability, thermophysical properties and heat transfer applications of nanofluid - a review, J. Mol. Liq. 364 (2022), 120034, https://doi.org/10.1016/J.MOLLIQ.2022.120034. Oct.

[12] G. Sriharan, S. Harikrishnan, H.F. Oztop, A review on thermophysical properties, preparation, and heat transfer enhancement of conventional and hybrid nanofluids utilized in micro and mini channel heat sink, Sustain. Energy Technol. Assess. 58 (2023), 103327, https://doi.org/10.1016/J.SETA.2023.103327. Aug.

[13] G. Coccia, S. Tomassetti, G. Di Nicola, Thermal conductivity of nanofluids: a review of the existing correlations and a scaled semi-empirical equation, Renew. Sustain. Energy Rev. 151 (2021), 111573, https://doi.org/10.1016/J.RSER.2021.111573. Nov.

[14] S. Javed, H.M. Ali, H. Babar, M.S. Khan, M.M. Janjua, M.A. Bashir, Internal convective heat transfer of nanofluids in different flow regimes: a comprehensive review, Physica A 538 (2020), 122783, https://doi.org/10.1016/J.PHYSA.2019.122783. Jan.

[15] Y. Xuan, W. Roetzel, Conceptions for heat transfer correlation of nanofluids, Int. J. Heat Mass Transf. 43 (19) (2000) 3701–3707, https://doi.org/10.1016/S0017-9310(99)00369-5. Oct.

[16] S.E.B. Maïga, C.T. Nguyen, N. Galanis, G. Roy, Heat transfer behaviours of nanofluids in a uniformly heated tube, Superlattices Microstruct. 35 (3–6) (2004) 543–557, https://doi.org/10.1016/J.SPMI.2003.09.012. Mar.

[17] M. Corcione, M. Cianfrini, A. Quintino, Two-phase mixture modeling of natural convection of nanofluids with temperature-dependent properties, Int. J. Therm. Sci. 71 (2013) 182–195, https://doi.org/10.1016/J.IJTHERMALSCI.2013.04.005. Sep.

[18] B.C. Pak, Y.I. Cho, Hydrodynamic and heat transfer study of dispersed fluids with submicron metallic oxide particles, Exp. Heat Transfer 11 (2) (1998) 151–170, https://doi.org/10.1080/08916159808946559.

[19] T.S. Krishnakumar, A. Sheeba, V. Mahesh, M.Jose Prakash, Heat transfer studies on ethylene glycol/water nanofluid containing TiO2 nanoparticles, Int. J. Refrigerat. 102 (2019) 55–61, https://doi.org/10.1016/J.IJREFRIG.2019.02.035. Jun.

[20] E.V. Timofeeva, J.L. Routbort, D. Singh, Particle shape effects on thermophysical properties of alumina nanofluids, J. Appl. Phys. 106 (1) (2009), 014304, https://doi.org/10.1063/1.3155999. Jul.

[21] R.L. Hamilton, Thermal conductivity of heterogeneous two-component systems, Ind. Eng. Chem. Fund. 1 (3) (1962) 187–191, https://doi.org/10.1021/I160003A005/ASSET/I160003A005.FP.PNG_V03. Aug.

[22] W. Yu, S.U.S. Choi, The role of interfacial layers in the enhanced thermal conductivity of nanofluids: a renovated Maxwell model, J. Nanopart. Res. 5 (1–2) (2003) 167–171, https://doi.org/10.1023/A:1024438603801/METRICS. Apr.

[23] X.Q. Wang, A.S. Mujumdar, Heat transfer characteristics of nanofluids: a review, J. Therm. Sci. 46 (1) (2007) 1–19, https://doi.org/10.1016/J.IJTHERMALSCI.2006.06.010. Jan.

[24] S.M.S. Murshed, K.C. Leong, C. Yang, Enhanced thermal conductivity of TiO_2—water based nanofluids, J. Therm. Sci. 44 (4) (2005) 367–373, https://doi.org/10.1016/J.IJTHERMALSCI.2004.12.005. Apr.

[25] M. Corcione, Empirical correlating equations for predicting the effective thermal conductivity and dynamic viscosity of nanofluids, Energy Convers. Manag. 52 (1) (2011) 789–793, https://doi.org/10.1016/J.ENCONMAN.2010.06.072. Jan.

[26] J. Buongiorno, et al., A benchmark study on the thermal conductivity of nanofluids, J. Appl. Phys. 106 (9) (2009), 094312, https://doi.org/10.1063/1.3245330. Nov.

[27] H.E. Patel, T. Sundararajan, S.K. Das, An experimental investigation into the thermal conductivity enhancement in oxide and metallic nanofluids, J. Nanopart. Res. 12 (3) (2010) 1015–1031, https://doi.org/10.1007/S11051-009-9658-2/TABLES/2. Mar.

[28] S. El Bécaye Maïga, S.J. Palm, C.T. Nguyen, G. Roy, N. Galanis, Heat transfer enhancement by using nanofluids in forced convection flows, Int. J. Heat Fluid Flow 26 (4) (2005) 530–546, https://doi.org/10.1016/J.IJHEATFLUIDFLOW.2005.02.004. Aug.

[29] J. Sarkar, A critical review on convective heat transfer correlations of nanofluids, Renew. Sustain. Energy Rev. 15 (6) (2011) 3271–3277, https://doi.org/10.1016/J.RSER.2011.04.025. Aug.

[30] Q. Li, Y. Xuan, Convective heat transfer and flow characteristics of Cu-water nanofluid, Sci. China Ser. E: Technol. Sci. 45 (4) (2002) 408–416, https://doi.org/10.1360/02YE9047. *2002 45:4*.

[31] Y. Xuan, Q. Li, Investigation on convective heat transfer and flow features of nanofluids, J. Heat Transfer 125 (1) (2003) 151–155, https://doi.org/10.1115/1.1532008. Feb.

[32] W. Duangthongsuk, S. Wongwises, An experimental study on the heat transfer performance and pressure drop of TiO2-water nanofluids flowing under a turbulent flow regime, Int. J. Heat Mass Transf. 53 (1–3) (2010) 334–344, https://doi.org/10.1016/J.IJHEATMASSTRANSFER.2009.09.024. Jan.

[33] M. Chandra Sekhara Reddy, V. Vasudeva Rao, Experimental investigation of heat transfer coefficient and friction factor of ethylene glycol water based TiO2 nanofluid in double pipe heat exchanger with and without helical coil inserts, Int. Commun. Heat Mass Transf. 50 (2014) 68–76, https://doi.org/10.1016/J.ICHEATMASSTRANSFER.2013.11.002. Jan.

[34] A.A. Permanasari, B.S. Kuncara, P. Puspitasari, S. Sukarni, T.L. Ginta, W. Irdianto, Convective heat transfer characteristics of TiO2-EG nanofluid as coolant fluid in heat exchanger, AIP Conf. Proc. 2120 (1) (2019) 50015, https://doi.org/10.1063/1.5115691/1024582. Jul.

[35] M.C.S. Reddy, V.V. Rao, Experimental studies on thermal conductivity of blends of ethylene glycol-water-based TiO_2 nanofluids, Int. Commun. Heat Mass Transf. 46 (2013) 31–36, https://doi.org/10.1016/J.ICHEATMASSTRANSFER.2013.05.009. Aug.

[36] K.A. Hamid, W.H. Azmi, R. Mamat, K.v. Sharma, Experimental investigation on heat transfer performance of TiO2 nanofluids in water-ethylene glycol mixture, Int. Commun. Heat Mass Transf. 73 (2016) 16–24, https://doi.org/10.1016/J.ICHEATMASSTRANSFER.2016.02.009. Apr.

[37] T. Zuccheri, M. Colonna, I. Stefanini, C. Santini, D. Di Gioia, Bactericidal activity of aqueous acrylic paint dispersion for wooden substrates based on TiO2 nanoparticles activated by fluorescent light, Materials (Basel) 6 (8) (2013) 3270–3283, https://doi.org/10.3390/MA6083270. *2013, Vol. 6, Pages 3270-3283*Aug.

[38] L.M. Sikhwivhilu, S.Sinha Ray, N.J. Coville, Influence of bases on hydrothermal synthesis of titanate nanostructures, Appl. Phys. A Mater. Sci. Process 94 (4) (2009) 963–973, https://doi.org/10.1007/S00339-008-4877-4/METRICS. Nov.

[39] R. Quesada-Cabrera, A. Mills, C. O'Rourke, Action spectra of P25 TiO2 and a visible light absorbing, carbon-modified titania in the photocatalytic degradation of stearic acid, Appl. Catal. B 150-151 (2014) 338–344, https://doi.org/10.1016/J.APCATB.2013.12.008. May.

[40] D.S. Udawattha, M. Narayana, U.P.L. Wijayarathne, Predicting the effective viscosity of nanofluids based on the rheology of suspensions of solid particles, J. King Saud Univ. Sci. 31 (3) (2019) 412–426, https://doi.org/10.1016/J.JKSUS.2017.09.016. Jul.

[41] 'Thermophysical Properties of Fluid Systems'. https://webbook.nist.gov/chemistry/fluid/(accessed May 11, 2023).

[42] O.A. Alawi, N.A.C. Sidik, H.W. Xian, T.H. Kean, S.N. Kazi, Thermal conductivity and viscosity models of metallic oxides nanofluids, Int. J. Heat Mass Transf. 116 (2018) 1314–1325, https://doi.org/10.1016/J.IJHEATMASSTRANSFER.2017.09.133. Jan.

[43] I. Gherasim, G. Roy, C.T. Nguyen, D. Vo-Ngoc, Experimental investigation of nanofluids in confined laminar radial flows, Int. J. Therm. Sci. 48 (8) (2009) 1486–1493, https://doi.org/10.1016/J.IJTHERMALSCI.2009.01.008. Aug.

[44] H.C. Brinkman, The viscosity of concentrated suspensions and solutions, J. Chem. Phys. 20 (4) (1952), https://doi.org/10.1063/1.1700493, 571-571Apr.

[45] H.W. Coleman and W.G. Steele, 'Experimentation, validation, and uncertainty analysis for engineers', p. 358, Accessed: May 11, 2023. [Online]. Available: https://www.wiley.com/en-us/Experimentation%2C+Validation%2C+and+Uncertainty+Analysis+for+Engineers%2C+4th+Edition-p-9781119417989.

[46] Y.A. Çengel, 'Heat and mass transfer : a practical approach', p. 901, 2007.